Intelligent Machining Methods for Ti6Al4V: A Review

Sílvia Ribeiro-Carvalho [1*], R. B. D. Pereira [2], Ana Horovistiz[1], J. Paulo Davim[1]

[1] Department of Mechanical Engineering, University of Aveiro, Campus of Santiago, 3810-193 Aveiro, Portugal; horovistiz@ua.pt (A. H.); pdavim@ua.pt (J.P.D.); tel.: (+351) 234 370 830

[2] Department of Mechanical Engineering, Centre for Innovation in Sustainable Manufacturing, Federal University of São João del-Rei, Praça Frei Orlando, 170, Centro, São João del Rei, 36.307-352, Brazil, robsondutra@ufsj.edu.br (R.B.D.P); tel.: (+55) 3233795879

[*]Correspondent author: sdrc@ua.pt (S. C.); tel.: (+351) 234 370 830

Abstract

Digital manufacturing is a necessity to establishing a roadmap for the future manufacturing systems projected for the fourth industrial revolution. Intelligent features such as behavior prediction, decision-making abilities, and failure detection can be integrated into machining systems with computational methods and intelligent algorithms. This review reports on techniques for Ti6Al4V machining process modeling, among them numerical modeling with finite element method (FEM) and artificial intelligence-based models using artificial neural networks (ANN) and fuzzy logic (FL). These methods are intrinsically intelligent due to their ability to predict machining response variables. In the context of this review, digital image processing (DIP) emerges as a technique to analyze and quantify the machining response (digitization) in the real machining process, often used to validate and (or) introduce data in the modeling techniques enumerated above. The widespread use of these techniques in the future will be crucial for the development of the forthcoming machining systems as they provide data about the machining process, allow its interpretation and quantification in terms of useful information for process modelling and optimization, which will create machining systems less dependent on direct human intervention.

Keywords: Intelligent machining methods; Ti6Al4V; Finite element method; Digital image processing; Artificial intelligence.

1 Introduction

The forthcoming manufacturing systems are a popular subject around the scientific and industrial sectors. Within this scope, digital manufacturing (DM), and its role in the fourth industrial revolution emerges has a topic of great relevance for the development of the smart machining systems [1, 2], as shown in Figure 1. It is important to mention that, in many production sectors, DM is already a well-implemented reality, where computer systems are responsible for monitoring and control manufacturing processes [1–3].

However, several characteristics, intrinsic to the machining process dynamics have contributed to delay in the introduction of digital technologies in machining operations, such as turning, milling, drilling [1]. An aspect worth mentioning is the multivariate character and complex interconnection between the entrance and response variables in machining operations, which makes the development of predictive models a challenging task [4]. Numerous authors developed experimental work to create statistical, artificial intelligence (AI) and hybrid models, as well as, to validate numerical models developed with the finite element method (FEM) [5]. FEM simulations have been parametrized, to generate digital twins of machining operations, to study the thermomechanical response during cutting and to select the best cutting settings for different combinations of materials and tools [6–8]. The artificial intelligence models, created using neural networks (NN), fuzzy logic and machine learning have been gaining popularity in the machining field, since they can predict variables, such as tool wear, tool life, surface roughness that are used to control the machining process and guarantee the quality of the machined components [9, 10]. AI-tools have been also used in the development of machining simulations, namely in the selection of the simulation parameters, but also in the optimization of cutting operations designed with FEM [11]. AI algorithms and machine learning are frequently behind the development of smart machining systems [12].

The integration of digital tools for monitoring and controlling machining operations is also and field that has to be developed in the scope of industry 4.0. In other manufacturing system, processes control can be achieved through monitoring systems, such as sensors and/or machine vision systems (MVS) that work along with process models that relate the system's current status with the required one [3, 13].

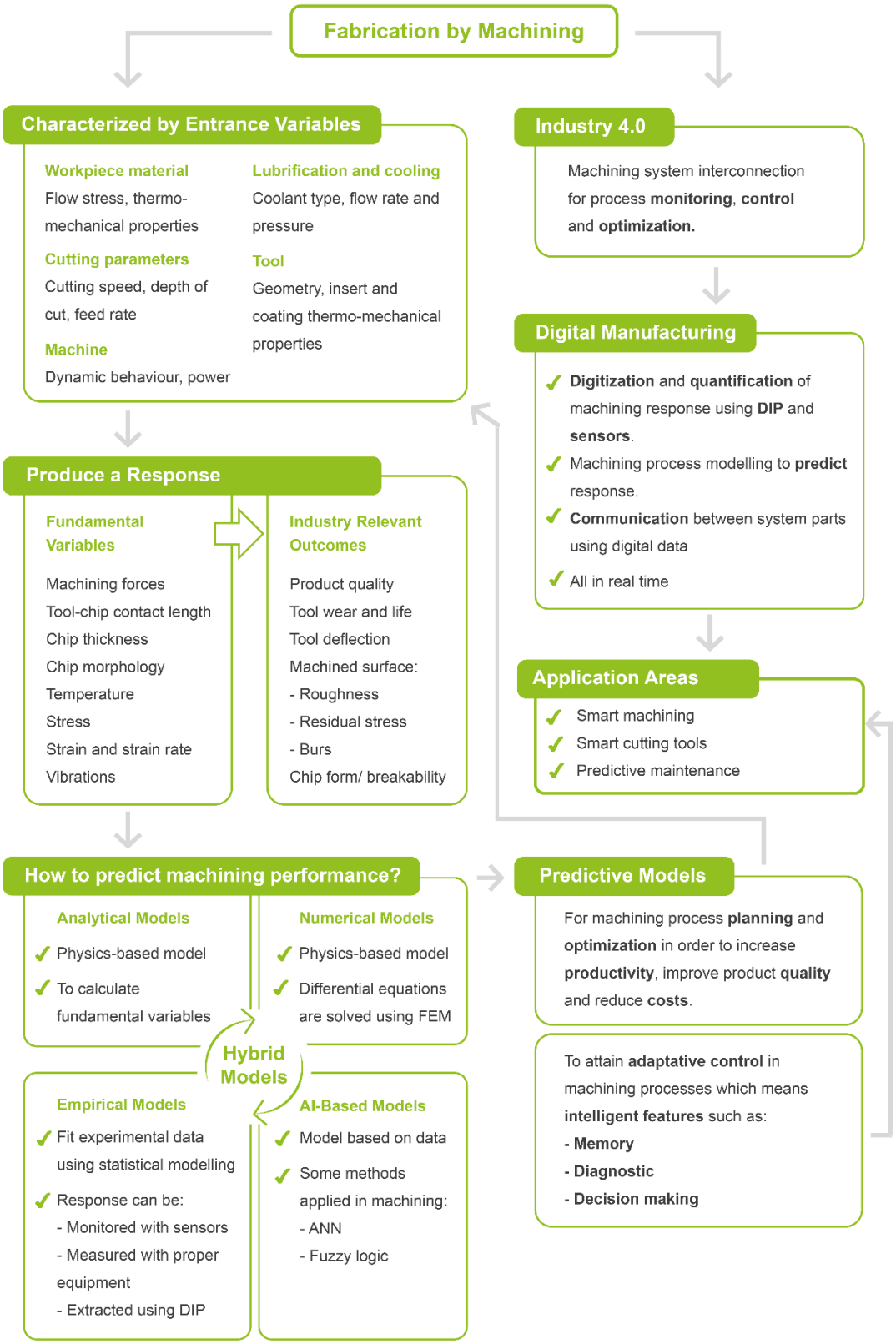

Figure 1. Components of an intelligent system.

Researchers have been using sensors, including, dynamometers, thermocouples, accelerometers, embedded in the machining system to study the process dynamics [14–17].The obtained signals (cutting forces, workpiece and tool temperature, vibration, and others) are then used to create machining models that relate the measurements with other variables, namely, tool wear, surface roughness, chip morphology [18–20]. The machining process dynamics can be also evaluated using machining simulations [21–23]. However, introduce conventional sensors, such as piezoelectric dynamometers, into machining systems results in high implementation costs, also, the equipment take time to install and are characterized by not being portable (they are typically attached into the tool holder or working table [24, 25]. To address to these limitations, a line of research in the field of intelligent machining consist in the development of smart cutting tools. Several authors reported the creation of smart cutting tools for cutting force measurement, using piezoelectric films [26], optical fibers [24], acoustic wave strain sensors [27], micro-electro-mechanical system strain gauge [25], the designed tools were characterized by having an equivalent performance and a lower cost when compared with conventional piezoelectric dynamometers.

In some manufacturing systems, online process monitoring, and control are achieved through MVS, which uses digital cameras to observe the process and apply algorithms to extract information from digital images to make decisions regarding the process [28]. Nevertheless, in machining, the region of interest is focused in the cutting zone, where the interaction between the tool and the workpiece occurs, as well as the formation of chips. However, this area can be difficult to observe due to the type of operation, the occurrence of wrapped metal chips, and the presence of lubricants that cover the cutting zone. Some authors have been using digital cameras to observe the cutting process in real-time [28] to evaluate the mechanism of metal chip formation [29], and the formed machined surface [9]. Yet, most reported works were conducted under dry conditions, in turning operations, with samples designed to allow the proper detection of the interest zone by the digital camera, which limits the use of such systems more widely.

It is important to highlight, that a digital image can be a reach source of information regarding the machining process, and while online acquisition systems are less common (but quite useful for digital manufacturing), offline observations of the cutting tools, metal chips, and machined surfaces have been explored by machining researchers for developing process models and study

aspects regarding the tool wear and life [30, 31], the morphology and microstructure of metal chips [23] and the integrity of machined surfaces (topography, microstructure, and others) [23, 30].

Given the state-of-art reported previously and considering that industry 4.0 intends to interconnect the manufacturing chain via the internet of things, it is necessary to convert relevant process information in digital data (digitization) to be used in process modeling, optimization, control and communication [32]. Digitizing and modelling the machining process is crucial to provide to the system the *"ability to correctly interpret external data, to learn from such data, and to use those learnings to achieve specific goals and tasks through flexible adaptation"* [33]. An intelligent machining system must has equivalent skills to those performed by an experienced operator including, monitoring, decision and diagnostic capabilities, required for an accurate response in different operating scenarios [1, 4]. As shown in Figure 1, decision and diagnostic capabilities rely on predictive process models that relate the entrance and response variables in machining operations [1]. If the conditions change, those models can predict the new working state, recognize failure, and relate faults and effects [4]. This arrangement of acquiring and applying knowledge is the key to an adaptively controlled machining system and for the development of smart machining techniques [4, 34].

The review scope is focused in computational tools for modelling, including FEM simulations to create machining process digital twins and AI algorithms to develop predictive models, as well as, in digital image processing techniques for digitizing the machining process. The intelligent, predictive, and digital character of these methodologies is in line with the requirements for industry 4.0 and smart machining implementation. The article mainly reports research work developed in Ti6Al4V titanium alloy, or techniques applied to other metallic alloys that can be used in different materials. Titanium alloy, such as Ti6Al4V have been used to produce high-value application in several industries, including naval, automotive, and biomedical. However, this material is known to be difficult-to-cut by machining, which arises the need of further investigation on methods to improve the maquinability and quality of the machined parts [35, 36].

Section 2 starts with a description of Ti6Al4V alloy in terms of properties and machining behavior. Section 3 is about Ti6Al4V machining simulations with FEM, the constitutive material models for

Ti6Al4V are presented in section 3.1, the friction models that explain the contact conditions at the tool-chip interface in Ti6Al4V machining are in section 3.2. In section 3.3, a summary table (Table 5) that contains the modeling strategies adopted by field researchers is presented, followed by the chapter major conclusions. Section 4 is dedicated to AI methods in the development of predictive models using Ti6Al4V machining data, section 4.1 is about ANN, section 4.2 describes the fuzzy logic theory, section 4.3 refers to the adaptive neuro-fuzzy inference system. In section 4.4 a summary table (Table 6) with the strategies used authors to create predictive models for Ti6Al4V machining process is presented, followed by the chapter major conclusions. Section 5 outlines the application of DIP to the digitization of machining outputs, a summary table (Table 7) was created to summarize relevant research work. In discussion and outlook section (section 6) the future research lines are debated considering the main conclusions of this investigation, also a summary table (Table 8) containing smart machining techniques and smart cutting tools developed by researcher is presented and discussed.

2 Thermo-mechanical properties and machining behavior of Ti6Al4V

Ti6Al4V is a biphasic titanium alloy, aluminum is the stabilizer of the alpha-phase, while vanadium is the beta-phase stabilizer [29, 37, 38]. Ti6Al4V alloy has been used by medical and aerospace industry since it presents good mechanical property combinations of high yield strength and resistance to corrosion and fatigue [35, 39, 40]. The processing steps behind Ti6Al4V alloy fabrication will produce a microstructure, characterized by the grain size, the alpha-beta-phase volume fraction and the phase morphology [35, 38, 41–43].

Consequently, under machining conditions, the mechanical properties and deformation behavior will occur differently according to the alloy microstructure [38, 41, 44]. In this context, Sun [41] carried out machining tests with Ti6Al4V alloys with different microstructural arrangements and evaluate how the chip formation and the cutting forces change for different cutting conditions. The authors reported that, for cutting speeds lower than 100 m/min, the cutting force was lower for the globular phase morphology when compared with bi-modal and lamellar. Those results match with the tendencies presented by Peters [38] that stated that coarse and lamellar arrangements have lower strength and ductility compared to fine and equiaxed morphologies. Consequently, the last

group of microstructures will be easier to cut and the expected cutting forces during machining will be lower [41, 44].

Yet, Ti6Al4V is known as a difficult-to-cut material due to its thermo-mechanical properties. Even at high-temperature Ti6Al4V has the capacity to maintain strength. Additionally, the plastic deformation that occurs during Ti6Al4V machining, promotes the workpiece strengthening due to work hardening effect, consequently, high cutting forces are expected in Ti6Al4V machining [40].

The metal chip produced during Ti6Al4V machining reveals information about the alloy deformation mechanism. For a wide range of cutting parameters, segmented chips occur in Ti6Al4V machining. Numerous authors explain this morphology with the occurrence of localized deformation mechanisms along with crack growth [45]. The adiabatic shear band is formed due to the coexistence of two opposite mechanisms, which are the material strain hardening and thermal softening effect, that alter the material resistance to plastic deformation [40]. Chip segmentation promotes the variation of the chip thickness, which induces higher cutting forces, tool vibration and chatter along with worst surface finishing [45, 46].

Another issue regarding Ti6Al4V machining is the high chemical affinity between the alloy and the available cutting tools. This phenomenon potentiates the tool wear rate, which reduces the dimensional accuracy of the machined part [40, 47].

Also, Ti6Al4V has a low thermal conductivity, which means that the heat at the cutting zone is not dissipated by either the workpiece or the metal chip, but by the cutting tool [47]. Therefore, the tool wear rate will increase along with a reduction in tool life. A worn-out tool will increase the specific cutting force and promote a worst machined surface finishing [40, 46, 47].

3 Numerical modeling of Ti6Al4V machining process using FEM

It is important to keep in mind that, whatever the purpose may be, predict outcomes or process optimize, to modeling machining, using the FEM, the models should be capable to replicate the Ti6Al4V behavior in real machining setups. For this reason, the results of analytical and empirical models are often entered into numerical simulations to validate them. For example, the experimental cutting forces can be used to analytically calculate the friction coefficient, which is an input for simulations [23, 29]. Then, the simulated and experimental forces can be compared,

in terms of deviations in order to validate the machining simulation. Machining modeling with FEM relies upon data from the workpiece, the cutting tool and the interaction between them, as shown in Figure 2.

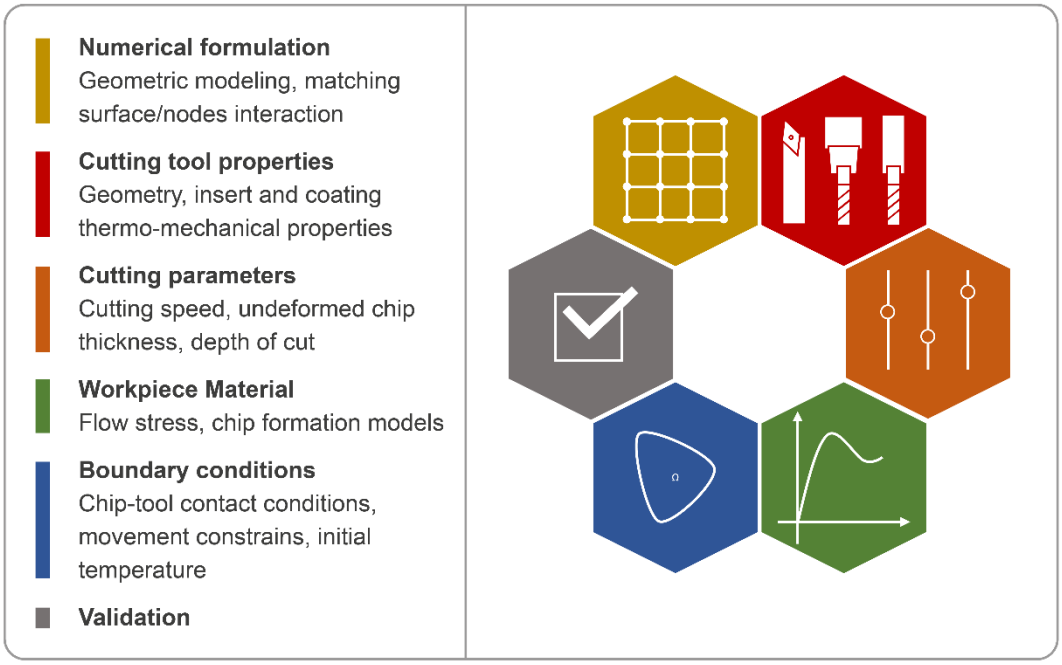

Figure 2. Machining modelling requirements using finite element method (FEM).

3.1 Phenomenological constitutive models for Ti6Al4V machining modeling

In machining, the cutting tool edge is pressed against the workpiece causing plastic deformation of the workpiece material, as well as, the physical separation of metal layers [48]. The deformation parameters, specifically strain, strain rate and temperature, will change along with the material flow stress behavior [49]. For this reason, the development of machining simulations requires a material flow stress model, that governs the response of the deforming material. The workpiece material model is critical data for machining simulations with FEM [36, 48] because it changes the system response in terms of cutting forces, temperature distribution and chip morphology [50]. The phenomenological models commonly used to simulate Ti6Al4V machining are presented in Table 1. Among them the Johnson-Cook (J-C) plasticity model [51], the modified J-C model presented by Calamaz [49] and the power viscosity law.

Table 1. Phenomenological constitutive models for machining modeling Ti6Al4V.

Johnson-Cook (J-C) Material Model [51]

$$\sigma = \left[A + B.\varepsilon_p^n\right]\left[1 + C.\left(\frac{\dot{\varepsilon}_p}{\dot{\varepsilon}_0}\right)\right]\left[1 - \left(\frac{T - T_0}{T_m - T_0}\right)^m\right] \quad \text{eq.1}$$

Flow stress = Strain hardening x Strain-rate (viscosity) x Thermal softening

Modified Johnson-Cook

$$\sigma = \left[A + B.\varepsilon_p^n.\left(\frac{1}{exp\left(\varepsilon_p^a\right)}\right)\right]\left[1 + C.\left(\frac{\dot{\varepsilon}_p}{\dot{\varepsilon}_0}\right)\right]\left[1 - \left(\frac{T - T_0}{T_m - T_0}\right)^m\right] h\left(\varepsilon_p, T\right)$$

$$D = 1 - \left(\frac{T}{T_m}\right)^d ;\ S = \left(\frac{T}{T_m}\right)^b$$

Flow stress = Strain hardening x Strain-rate (viscosity) x Thermal softening x Strain softening

Proposed by Calamaz [49]

$$h\left(\varepsilon_p, T\right) = \left[D + (1 - \mathrm{D}).\tanh\left(\frac{1}{\varepsilon_p + S}\right)^c\right]; \quad \text{eq.2}$$

Proposed by Sima & Ozel [52]

$$h\left(\varepsilon_p, T\right) = \left[D + (1 - \mathrm{D})\tanh\left[\tanh\left(\frac{1}{\left(\varepsilon_p + S\right)^e}\right)^f\right]\right]; \quad \text{eq.3}$$

Adaption of the Ludwick hardening term of Harzallah *et al*. [53]

$$\sigma = A(\dot{\varepsilon}, T) + B(\dot{\varepsilon}, T).{\varepsilon_p}^{n(\dot{\varepsilon}, T)} \quad \text{eq.4}$$

Flow stress = yield strength x hardening modulus x hardening coefficient

Power Viscosity Law [54]

$$\sigma = g\left(\varepsilon_p\right).\Gamma\left(\dot{\varepsilon}_p\right).\Theta(T) \quad \text{eq.5}$$

$$g\left(\varepsilon_p\right) = \sigma_0\left[1 + \frac{\varepsilon_p}{\varepsilon_0}\right]^{\frac{1}{n}};\ \Gamma\left(\dot{\varepsilon}_p\right) = \left[1 + \frac{\dot{\varepsilon}_p}{\dot{\varepsilon}_0}\right]^{\frac{1}{m}};\ \Theta(T) = c_0 + c_1.T + \cdots$$

σ: flow stress; ε_p: plastic strain; $\dot{\varepsilon}_p$: plastic strain rate; ε_0: reference plastic strain; $\dot{\varepsilon}_0$: reference plastic strain rate; T: absolute temperature; T_0: reference temperature; T_m: absolute melting temperature; A, B, C, m, n, a, b, c, d, e, f: empirically determined model parameters.

3.1.1 Johnson-Cook material & damage model

The J-C flow stress is calculated considering the coupled effects of the material strain hardening (Ludwick hardening term), the strain-rate dependency and the material thermal softening (equation 1). The J-C model was adopted by authors [36, 47, 48, 50, 53, 55, 56] to simulate Ti6Al4V machining. To obtain the model parameters, mechanical tests, such as Hopkins pressure bar testing are required to empirically fit the stress-strain curves into the model [57–62]. Those tests are performed under high strain, strain rate and temperature to replicate what happens to

he material under machining conditions [36, 53, 63]. Table 2 contains the J-C parameters often used for different Ti6Al4V machining.

Despite being widely employed, the J-C model presents a few downsides, one of them being the inaccuracy for strain rates above $10^3\ s^{-1}$ and strains beyond 0.3, which are achieved in industrial machining [49]. Additionally, the model does not capture the shear banding that occurs in Ti6Al4V chips [49, 64]. To address this limitation, the J-C model is typically implemented with a damage criterion. Table 2 contains two material damage criteria used in Ti6Al4V machining simulations, the J-C damage model and Cockroft and Latham (C-L) fracture model [65], both models can be used to obtain the serrated chips in Ti6Al4V machining simulations.

To apply the J-C damage model it is necessary to calculate the plastic strain (equation 6), then, the plastic strain value is updated in equation 7, when W_D reaches the value 1, the damage initiation occurs. In simulation environment, this means that the separation of the metal chip from the cutting tool-workpiece interface happens when the deformation parameters (strain and stress) at cutting insert tip node are greater than the values supported by the workpiece material [50, 55].

The C-L damage criterion, shown in equation 8, is a fracture criterion that describes the conditions in which deformation leads to material fracture, the model relates the mechanism responsible for crack formation (chip segmentation) to the material tensile stress state. The C-L damage model was used by several authors to describe Ti6Al4V chip formation [36, 49, 66, 67].

Table 2. J-C model parameters and damage models for Ti6Al4V machining operations

Process	A (MPa)	B (MPa)	C	n	m	Obtained from
Orthogonal Cutting Syed 2004 [68]	1098	1092	0.014	0.93	1.1	Lesuer 2000 [57]
Orthogonal Cutting Calamaz 2008 [49]	968	380	0.0197	0.421	0.577	Li 2006 [69]
Orthogonal Cutting Sekar 2011 [66]	782.7	498.4	0.028	0.28	1	Lee & Lin 1998 [58]
	987.8	761.5	0.0152	0.4143	1.516	Ozel & Karpat 2007 [59]
	1104	1036	0.0139	0.6359	0.779	Khan *et al.* 2004 [60]
	1098	1092	0.014	0.93	1.1	[57]

Milling 3D Bajpai 2014 [55]	1098	1092	0.014	0.93	1.1	[57] Özel & Zeren 2004 [70]
Orthogonal Cutting Ducobu 2014 [45]	862	331	0.012	0.34	0.8	[57, 70] Sun & Guo 2009 [71]
Helical Cutting Ji 2015 [56]	880	331	0.012	0.8	0.34	-
Orthogonal Cutting Zhang 2015 [47]	862	331	0.012	0.34	0.8	[57]
	1098	1092	0.014	0.93	1.1	
Face Milling Niesłony 2015 [72]	500	864	0.01594	0.196	0.605	-
Orthogonal Cutting & Turning Niesłony 2015 [73]	968	380	0.0197	0.421	0.577	[69]
Orthogonal Cutting Harzallah 2017 [53]	880	582	0.041	0.35	0.63	Harzallah 2017 [53]
High speed machining (2D) Li 2017 [50]	782	498	0.028	0.28	1	[58]
Broaching Ortiz-de-Zarate 2018 [36]	1130	530	0.0165	0.39	0.61	-
Drilling 3D Parida 2018 [48]	880	331	0.012	0.8	0.34	

A: initial yield stress; B: hardening modulus; C: strain rate dependency coefficient; n: strain hardening coefficient; m: thermal softening coefficient;

J-C damage model

$$W_D = \sum \frac{\Delta \varepsilon_p}{\varepsilon_{p_D}} \qquad \text{eq.6}$$

$$\varepsilon_{p_D} = \left[d_1 + d_2 e^{\left(d_3 \frac{\sigma_n}{\sigma_{mises}} \right)} \right] \left[1 + d_4 \ln\left(\frac{\dot{\varepsilon}_p}{\dot{\varepsilon}_0} \right) \right] \left[1 + d_5 \frac{T - T_0}{T_m - T_0} \right] \qquad \text{eq.7}$$

Cockroft and Latham (C-L) fracture model [65]

$$\int_0^{\varepsilon_f} \sigma_{max} \, d\varepsilon_p = \mathrm{D} \qquad \text{eq.8}$$

W_D: J-C damage parameter; $\Delta\varepsilon_p$: plastic strain increment; ε_{pD}: plastic strain at damage initiation; σ_n: hydrostatic pressure; σ_{mises}: Mises stress; ε_f: limit failure strain; σ_{max}: maximum principal stress; d_1, d_2, d_3, d_4, d_5: failure parameters of J-C damage model; D: C-L damage value.

3.1.2 Other relevant material models for Ti6Al4V machining simulations

The Hyperbolic TANgent law (TANH) proposed by Calamaz [49] is shown in equation 2 and is an adaptation to the J-C law. The model adds up the strain-softening effect into the original J-C

model, in order to account with the dynamic recrystallization effect that happens when the workpiece material is deformed in machining operations [49, 64]. The THAN term captures the softening effect that happens at high strain and strain rates, thus the shear banding that happens in Ti6Al4V metal chips is captured by the model without any damage model [49]. The model parameters A, B, C, m, n have the same meaning as for J-C model a, b, c, d are the new material constants for TANH law. Sima and Özel [52] also developed a TANH model inspired by the one proposed by Calamaz [49], this new model adds a new parameter that allows further control of the softening effect. Harzallah *et al*. [53] proposed a flow stress model which is an adaption of the Ludwick hardening term (strain hardening), the formulation is demonstrated in equation 4. The coupling between strain rate and temperature is allowed through the material parameters, that were calculated with dynamic compression tests.

3.2 Contact and friction models for Ti6Al4V machining modeling

Frictional models are complex, however crucial in machining simulations since they describe the interactions at the tool-chip interface. Aspects such as stress distribution, in machined surface and cutting tool, strain and cutting temperature will increase with severe tool-chip frictional conditions [74]. For this reason, lubrification and or cooling strategies are used when machining Ti6Al4V to improve the contact conditions [75–77]. In machining operations where the friction conditions are extreme, more energy is required to cut and higher tool wear rate is expected, reducing the tool life and the integrity of the machined part [5, 50, 64].

One of the first approaches to modeling friction in machining FEM models was to use Coulomb's friction law. Accordingly to this model (equation 9 from Table 3), the frictional shear stress (τ_f) on the tool rake face is proportional to the normal stress (σ_n) where the coefficient of proportionality is the coefficient of friction (μ). However, several authors agree that the friction in the rake face is not constant along with its extension and is a function of normal and frictional stress distributions [78].

Table 3. Friction models for Ti6Al4V machining simulations.

Coulomb friction law				
$\tau_f = \mu\sigma_n$				eq.9
Shear friction				
$\tau_f = m.k$				eq.10
Zorev's stick-slip model [79]				
$\tau_f(x) = \tau_y$	when	$\mu.\sigma_n(x) \geq \tau_y$ $0 < x < l_p$	**Cohesive or sticking**: near cutting edge, tool tip.	eq.11
$\tau_f(x) = \mu.\sigma_n(x)$	when	$\tau_f < \tau_y$ $l_p < x \leq l_c$	**Slip or sliding**: towards the end of the contact.	
Coulomb-Tresca friction model				
if $\mu\sigma_n = \tau_y$	$\tau_f = \tau_y$	$\tau_y = m.k$	**Cohesive or sticking**: near cutting edge, tool tip.	eq.12
if $\tau_f < \tau_y$	$\tau_f = \mu\sigma_n$		**Slip or sliding**: towards the end of the contact.	

τ_f: frictional shear stress; μ: coefficient of friction; σ_n: tool-chip normal stress; τ_y: shear stress of the material; l_p: transitional zone; l_c: tool-chip contact length; m: friction factor, k: work material shear flow stress.

Zorev [79] proposed a friction law (equation 11), to modeling the contact at the chip-tool interface conditions in terms of normal and shear stress distribution. The model considers that the contact conditions at the chip-tool interface change along the contact length (l_c), where two main regions are considered, a sticking and a sliding zone [53]. The cohesive or sticking contact occurs near the edge radius, in this region, the frictional stress is equal to the chip material ultimate shear stress, while, at the sliding region the friction stress is calculated with the Coulomb friction law. Other authors, implemented the friction models in FEM based on classic friction models such as the Coulomb friction model and the Tresca friction model (shear friction model) as demonstrated in equation 12 [49]. The Ti6Al4V friction models as well the constants are presented in Table 3 and Table 4 respectively, for different machining operations under different cutting conditions.

Table 4. Friction coefficient for several machining operations in Ti6Al4V alloy.

Machining process	Friction model & Lubrifaction-Cooling	Cutting speed [m/min]	μ	m
Orthogonal Cutting Syed 2004 [68]	Coulomb Dry	10-100	0.3, 0.5, 0.7, 0.8	-
Orthogonal cutting Calamaz 2008 [49]	Coulomb-Tresca Dry	60,180	0.05, 0.3	1, 0.5
Orthogonal cutting 2D Sima & Ozel 2010 [52]	Rake face split in 3 zones Dry	121.9, 240.8	**sticking** m=1; **shear friction** m= 0.85-0.9; **sliding** μ= 0.5	
Orthogonal cutting 2D & Turning 3D Ozel & Sima [80]	as in [52]; Dry	120	**2D:** as in [52]	
	Only shear friction Dry	100	**3D:** m= 0.85-0.9	
Orthogonal Cutting Sekar 2011 [66]	Coulomb Dry	24, 40, 61, 93	0.3	
Orthogonal Cutting Chiappini 2014 [67]	Shear friction Dry	40	-	0.7
Milling Bajpai 2014 [55]	Coulomb Dry	25, 50	0.6	-
Orthogonal Cutting Ducobu 2014 [45]	Coulomb Dry	75	0.05	-
Helical Milling Ji 2015 [56]	Coulomb Cold air	47, 63, 79, 94	0.5	-
Orthogonal Cutting Zhang 2015 [47]	Coulomb	90	0.2	-
Face Milling Niesłony 2015 [72]	Coulomb	80	0.5	-
Orthogonal Cutting Joshi 2015 [23]	Coulomb; At room temperature; Liquid Nitrogen; with heating	23.4, 91.8	0.62	-
Orthogonal Cutting Harzallah 2017 [53]	Coulomb-Tresca	15, 25	0.2	-
High speed machining (2D) Li 2017 [50]	Coulomb-Tresca	80, 120, 160	-	-
Broaching Ortiz-de-Zarate 2018 [36]	Stick-Slip Dry	2.5, 7.5	0.7	1
Drilling Parida 2018 [48]	Coulomb	25, 45, 60	0.6	-

3.3 Finite element modeling for Ti6Al4V machining: strategies, goals & challenges

Table 5 summarizes strategies, along with the researcher's goals in developing Ti6Al4V machining simulations. It can be observed that an accurate FEM machining model must guarantee a satisfactory prediction of the chip morphology, as well as a good estimative of the forces generated in real machining operations.

To validate those models, the process outputs are quantified with other methodologies such as empirical and (or) analytical modeling and compared with the values obtained with FEM [36, 47, 80, 81, 49, 50, 52, 53, 55, 66–68]. Authors often carry out experiments or refer to other researcher's work [45, 68] to compare the digital images of metal chips with the ones simulated. The digital images of the metal chips are collected from machining operations and morphological features, such as peaks, valleys are extracted using DIP techniques [49, 50, 52, 66, 67, 80, 82, 83]. Most of the machining models found for the Ti6Al4V alloy were developed and validated assuming dry conditions (Table 4), however, several cooling and lubrification strategies (MQL, cryogenic, cooled air) are used in industrial Ti6Al4V machining to improve the alloy machinability. Given this, it is important to create more Ti6Al4V machining models that include the influence of lubrification. This is a challenging task as it is necessary to translate the Ti6Al4V machining behavior when using lubrification strategies into parameters that can be parameterized in the FEM software.

Another important conclusion is that most of the FEM simulations were developed to calculate fundamental variables such as the ones described in Figure 1. Firstly, because some of those outputs are needed to validate simulations and sometimes because those outputs are difficult to measure accurately through experimental trials. However, authors such as Ozel & Sima [80] proposed a numerical model to predict tool wear, based on the adhesive wear model proposed by Usui *et al.* [84]. The authors used digital images of the worn-out tool to validate the proposed model. Other authors used the response variables measured with FEM to enter data into analytical models. For example, Zanger and Schulze [85] performed and validated a series of numerical simulations to obtain the state variables that influenced the tool wear during Ti6Al4V machining (for instance, stress, temperatures, chip contact, chip velocity) accordingly to analytical wear models. Then, the response variables were used to parameterize those analytical models.

Bai in 2017 [81] used simulations in FEM to validate an analytical model of chip formation for Ti6Al4V, the model was able to predict the formation of segmented and continuous chip depending on the material machining conditions. This type of model can be very useful in the future machining systems since allows the optimization of cutting parameters based on the characteristics of the metal chip. Seems that the hybrid, numerical-analytical, numerical approach can be useful in order to reduce the computation time especially in 3D simulations.

Another approach may be the one proposed by *Li et al.* [50] where the authors obtained the plastic strain, strain rate and temperature using FEM in order to use the collected data to enter into a microstructural texture simulator, called visco-plastic self-consistent (VPSC) to predict microstructural features of the machined surface resulting from machining processes.

Table 5. FEM strategies for several machining operations in Ti6Al4V.

Machining process	Material & damage & friction model; software; numerical formulation	Numerical outputs	Experimental outputs
Orthogonal Cutting Syed 2004 [68]	**Material:** J-C (eq.1) **Damage:** Recht's shear failure criterion [86] **Friction:** Coulomb (eq.9); AdvantEdge 2D**;** LAG	Plastic strain Temperature Machining forces Chip morphology	Not experimental, but from [20, 87, 88] Machining forces Chip morphology
Orthogonal cutting Calamaz 2000 [49]	**Material:** J-C (eq.1) , TANH (eq.2); **Material & Damage:** J-C (eq.1) + C-L (eq.8); **Friction:** C-T (eq.12) Forge 2D	Chip morphology Machining forces Plastic strain Temperature	Chip morphology Machining forces
Orthogonal cutting 2D Sima & Ozel 2010 [52]	**Material:** J-C (eq.1); TANH (eq. 2); Sima & Ozel (eq.3) **Friction:** sticking m=1 shear: m= 0.85/0.9 sliding: μ= 0.5 Deform 2D; LAG	Chip morphology & thickness Machining forces Strain Chip temperature	Chip morphology & thickness Machining forces
Orthogonal cutting 2D &Turning 3D Ozel & Sima 2010 [80]	**Material:** Sima & Ozel (eq.3) **Friction: 2D:** same as [52]**;** **3D:** eq.10 Deform 2D/3D; LAG	**2D/3D:** Machining forces; **2D:** Chip: peak & valley, Strain; **3D:** Tool & chip temperature, tool wear rate	**2D/3D:** Machining forces; **2D:** Chip: peak, valley; **3D:** tool wear rate
Orthogonal Cutting Sekar 2011 [66]	**Material:** J-C (eq.1) **Damage:** C-L (eq.8) **Friction:** Coulomb (eq.9); Deform 2D; LAG	Chip morphology, Cutting & feed forces, Stress & strain, Chip temperature	Cutting & feed forces, Chip morphology: peak, valley, pitch, compression ratio
Orthogonal Cutting Chiappini 2014 [67]	**Damage:** C-L (eq.8) Deform 2D **Friction:** eq.10 Deform 2D; LAG	Machining forces Chip: peak, valley, spacing, thickness, Cutting & tool temperature	Machining forces Chip: peak, valley, and thickness Temperature (thermocouple)
Milling Bajpai 2014 [55]	**Material:** J-C (eq.1) **Damage:** J-C (eq.6 & 7) **Friction:** Coulomb (eq.9) Abaqus explicit 3D	Cutting forces Chip: size & shape	Cutting forces Chip: size & shape
Orthogonal Cutting Ducobu 2014 [45]	**Material:** TANH (eq.2) + ALE J-C (eq.1) + LAG TANH (eq.2) + LAG **Friction:** Coulomb (eq.9); Abaqus explicit 2D	Chip formation Cutting forces Stress Chip temperature	Not experimental, but from literature: Cutting forces [89], Chip morphology [82, 89]
Helical Milling Ji 2015 [56]	**Material:** J-C (eq.1) **Damage:** J-C (eq.6 & 7) **Friction:** Coulomb (eq.9) Abaqus explicit 3D; LAG	Machining forces Chip morphology: peak, valley, pitch; Stress distribution	Machining forces Chip morphology: peak, valley, pitch

Orthogonal Cutting Zhang 2015 [47]	**Material:** J-C (eq.1) **Damage:** J-C (eq.6 & 7) **Friction:** Coulomb (eq.9); Abaqus explicit 2D ALE, LAG, CEL	Chip: geometry, compression ratio Machining forces Plastic deformation Temperature	Chip: geometry, compression ratio Machining forces
Face Milling Niesłony 2015 [72]	**Material:** J-C (eq.1); P-L (eq. 5) **Friction:** Coulomb (eq.9) AdvantEdge 3D; LAG	Machining forces Temperature	Machining forces Temperature (infrared camera)
Orthogonal Cutting & Turning Niesłony 2015 [73]	**Material:** J-C (eq.1); P-L (eq. 5) AdvantEdge 2D/3D; LAG	Residual stress sublayer (available in AdvantEdge)	Residual stress sublayer (X-ray diffraction)
Orthogonal Cutting Joshi 2015 [23]	**Material:** J-C (eq.1); **Damage:** C-L (eq.8); **Friction:** Coulomb (eq.9) Deform 2D; LAG implicit	Chip morphology Cutting temperature	Temperature; Chip morphology; Microstructure, Residual stress; Cutting forces
Orthogonal Cutting Harzallah 2017 [53]	**Material:** J-C (eq.1) Modified J-C (eq.4) **Damage:** J-C (eq.6 & 7) **Friction:** C-T (eq.12) Abaqus explicit 2D; LAG	Machining forces Chip geometry Strain Cutting temperature	Machining forces Strain Chip length Shear angle (from images captured in real-time)
High-speed machining 2D Li 2017 [50]	**Material:** J-C (eq.1) **Damage:** J-C (eq.6 & 7) **Friction:** C-T (eq.12) Abaqus explicit 2D; LAG	Machining forces Plastic strain & rate Temperature Chip morphology: peak, valley, spacing	Machining forces Chip morphology: peak, valley, spacing
Orthogonal Cutting Bai 2017 [81]	**Material & Damage:** TANH (eq. 2)	Shear stress Tool-chip: strain and temperature Chip morphology	Analytical [81] & empirical model to obtain: tool-chip contact length, friction, shear angle, machining forces, chip segmentation
Broaching Ortiz-de-Zarate 2018 [36]	**Material:** J-C (eq.1) **Damage:** C-L (eq.8) **Friction:** S-S (eq.11) Deform 2D; LAG implicit	Machining forces Chip morphology Residual stress	Surface roughness Surface topography Machining forces Chip morphology Residual stress Microstructural damage
Drilling Parida 2018 [48]	**Material:** J-C (eq.1) **Friction:** Coulomb (eq.9) Deform 3D; LAG	Drill bit temperature, Stress & strain Thrust force Torque Circularity	Surface roughness Thrust force Torque Circularity

J-C: Johnson-Cook; C-L: Cockroft-Latham; C-T: Coulomb-Tresca; ALE: Arbitrary Eulerian-Lagrangian; CEL: Coupled Eulerian-Lagrangian; LAG: Lagrangian; S-S: sticking and sliding model Zorev's.

4 Artificial intelligence-based modeling for Ti6Al4V machining process

The two main strategies considered in this review are the artificial neural network (ANN) and the fuzzy logic theory, as both methods have been used in modeling Ti6Al4V machining. Through these methods, it is possible to create models that relate the entrance variables with the generated response along with the possibility to create machining predictive models [90].

4.1 Artificial neural networks to predict Ti6Al4V machining response

An ANN also called neural network (NN) is a model inspired in the structure and functioning of the human nervous system. Regarding its operation, the artificial neuron receives signals from the previous neurons and emits signals to the following neurons. The strength of the neurons' connections is achieved by multiply each input by a suitable value of weight. Afterward, a scalar value called bias is added up into the total strength of inputs to determine the neuron activation tendency. The output signal is calculated with a nonlinear threshold function. The adjustment of weight and bias is made to reduce the error between predicted and the training data [4, 90].

The neurons in a NN are organized in layers and there are different structures for NN, one of the best known is the feed-forward NN, its main characteristic is that each layer has full interconnection with the next layer but never with neurons from the same layer. Multi-layered perceptron (MLP) and the radial basis function (RBF) neural network are two feed-forward NN topologies, the difference between them is associated with the calculations in the hidden layer [4, 90]. For MLP a sigmoidal activation function is applied to the product of inputs and weights, this network is typically trained with backpropagation (BP) algorithm [90]. The RBF neural network has only weights between the hidden layer and the output layer. A Gaussian activation function is applied to the Euclidean distance between inputs and centers (each neuron of the hidden layer is a center). RBF neurons are activated when the center is equal to the input [4].

The NN intelligence is acquired during the training phase, a BP algorithm is usually used to do that. Through an iterative process, the weights and biases are adjusted in the network until an input pattern produces a target output with a suitable error. Because of the characteristics mentioned before, this type of training is called supervised, the network has access to exemplars of both input and output patterns and the data is called training dataset. Both MLP and RBF are

supervised neural networks. The efficiency of prediction depends on factors such as the type of algorithm and the number of hidden layers, neurons, input and outputs [91, 92].

Several authors applied neural networks, with different in order to modeling machining operations with Ti6Al4V and predict response variables [90, 93, 94].

Upadhyay *et al.* [93] used a NN to predict the surface roughness in a Ti6Al4V turning considering the cutting conditions along with the vibration measured during experimentation. Two statistical models based on multiple regression analysis were created. The first one, related the measured surface roughness with the 3 components of the vibration signals, while the second model correlated the surface roughness with both cutting conditions and vibration signals. The authors used the results from the statistical predictive models to define the neural network configuration in terms of inputs since they concluded that modeling only with vibration signals led to higher error than using both vibration signals and cutting parameters.

Rajaparthiban and Sait [94] also create NN in order to predict surface roughness and material removal rate in Ti6Al4V turning. The authors conducted experiments to study the interactions between the cutting parameters and the response variables using the ANOVA. The statistical method provided information to optimize the cutting conditions in order to minimize the surface roughness and maximize the material removal rate. The work developed by these authors [93, 94] highlights the importance to know the interaction between machining variables to parameterize a NN.

Mello *et al.* [90] also used NN to predict two surface roughness parameters in Ti6Al4V turning. The authors used different NN, namely, MLP, RBF and SW-ELM (combines wavelet activation function with an ANN) in order to compare the performance of each technique in predicting surface roughness. They concluded that SW-ELM achieved the best prediction accuracy along with a smaller training time. The SW-ELM method uses two activation functions in the hidden layer and for this reason, is better to deal with non-linear transformations.

4.2 Fuzzy logic theory to predict Ti6Al4V machining response

In classical set theory, an element is a member of a set or not. In the fuzzy logic (FL), the membership grade of an element can be any value in the closed interval [0,1]. An element in a

set can have full membership (1), non-full membership grade (0) and partial membership if the membership grade is between 0 and 1 [4]. The fuzzy rules are a set of if-then statements that create an association between the input and output space [95]. In machining, a fuzzy rule can be a statement like *"If the feed is low and the cutting speed is low, then the surface roughness is medium"* [4, 96], the rules can be established based on human experience or based on empirical and statistical data.

For a Ti6Al4V drilling operation, Kumar and Baskar [96] applied fuzzy logic theory to create two empirical models, one using fuzzy logic and other using fuzzy logic associated with a statistical method called response surface methodology (RSM). To create the models, the authors executed experimentation for measuring the forces along with the surface roughness considering. The authors used the data from the FL model as input in the response surface methodology (RSM) to understand the relationship between the entrance and the response variables. They concluded that the hybrid approach FL-RSM was more effective to predict the output variables.

4.3 Adaptive neuro-fuzzy inference system to predict Ti6Al4V machining response

The adaptive neuro-fuzzy inference system (ANFIS) is a hybrid approach composed of a feed-forward NN which has a layer with neuro-fuzzy system [97]. The NN has good learning ability, however, the actions inside the neurons are *"black-boxes"* that the user cannot control. On the other hand, the FL theory is a tool to define criteria based on fuzzy rules, which is helpful for the decision making processes inside the network. Each neuron receives the input and produces a membership grade for that input because the neuron contains a membership function [4].

With experimental data of a Ti6Al4V turning process, Harsha *et al.* [91] apply and compare the performance of two AI-based modeling techniques, a feed-forward NN and a neuro-fuzzy (ANFIS) approach considering three inputs (cutting speed, feed rate and cutting time) and two outputs (roughness and tool wear). The results indicate that the second technique was more accurate to predict the tool wear and roughness because of the non-linearity presented between inputs and outputs.

Eduardo *et al.* and Geronimo *et al.* used ANN, namely MLP and MLP and ANFIS to modeling a Ti6Al4V drilling operation [98, 99]. The signals from several sensors, including acoustic emission sensors, three-dimensional dynamometer, and Hall effect sensor were collected during a drilling

operation. The in-process data along with the hole diameter and the surface roughness were used to develop and train the networks. Both studies claim the high accuracy of the methods to predict the hole diameter and hole roughness in drilling operations. The authors also stated that the methodology could be viable for control the cutting parameters in the drilling process accordingly with the output requirement, but also, that the implementation of such systems in the industry does not present much investment or changes in the equipment to be monitored [99].

4.4 Artificial intelligence models for Ti6Al4V machining: strategies, goals & challenges

From Table 6 it was possible to understand that authors explore AI-based models to study aspects regarding the machined surface integrity, such as surface roughness and geometrical accuracy. While others, create models to predict aspects regarding the tool wear and life. The machining output prediction provided by this modeling methodology is clearly of great industrial interest.

AI-based models, namely the NN are frequently trained with data obtained with experiments. This means that the network has access to a training dataset that contains entrance and response outputs, which usually indicates that a high volume of experimental trials must be performed, to obtain machined parts and worn tools. The response variables used to enter data into these AI models, can be measured using specific equipment, for example, the surface roughness is often quantified with profilometers and in some cases by extracting texture features from digital images of the machined surface, in order to create empirical models and or intelligent algorithm models to predict the surface roughness based on image features [9, 100]. The tool wear is generally measured using digital images from the cutting tools or using intelligent algorithm models as described before (this will be discussed in detail in section 5) [9].

A major setback for this technique is the amount of data needed to properly train and test an ANN, this may mean that intensive experimental and numerical work must be done in order to collect the process response variables [101]. The extensive application of these techniques should entail creating more partnerships between industrial application specialists and researchers to obtain that data from manufacturing systems that operate daily. A well-calibrated AI model has the capability to predict the machining response based on new input data which is very useful considering the demands for future machining systems and have high potential to make in-process response estimation conceivable.

Table 6. AI-based models for Ti6Al4V machining process.

Operation Author	Method	Architecture	Training algorithm	Input neurons	Output neurons
Turning Upadhyay *et al.* 2013 [93]	Neural Network	Three layers, one hidden layer with five neurons	BP with Levenberg–Marquardt algorithm	Cutting speed Feed rate, Depth of cut Vibration	Roughness
Turning Mello *et al.* 2017 [90]	Neural Network	MLP: sigmoidal function	289 data (85% train + 15% test)	Cutting speed Feed rate Depth of cut Flank wear Tool vibrations	Roughness (R_a and R_t)
		RBF: Gaussian function	fuzzy C means to calculate the centers		
		SW-ELM: two activation function inverse hyperbolic sine and Morlet wavelet			
Turning Harsha *et al.* 2018 [91]	Neural Network	Feed-forward three layers, one hidden layer with ten neurons	BP, data set 27 (train) + 8 (test)	Cutting speed Feed rate Cutting time	Flank tool wear; Roughness
	FL	"Gbell" membership function three rules for each parameter			
Turning Rajaparthiban and Sait 2018 [94]	Neural Network	Multi-layer (MPL) feed-forward ANN with one hidden layer with 10 neurons	BP	Cutting speed Feed rate Depth of cut	Roughness; Material removal rate
Turning Caggiano 2018 [18]	Neural Network	Three-layer cascade forward backpropagation ANN	BP with Levenberg–Marquardt algorithm	Vibration Force Acoustic emission	Tool wear
Drilling Eduardo *et al.* 2013 [98]	Neural Network	MLP: three hidden layers Transfer function: -hidden layer: tansig; -output layer: purelin;	BP, feed-forward algorithm (data: 60% train, 20% validation, 20% test)	Spindle speed Feed velocity Acceleration Acoustic emission Electrical power X, Y, Z force Signal from sensors	Maximum diameter Minimum diameter Surface roughness
Drilling Geronimo *et al.* 2013 [99]	Neural Network	MLP, Transfer function: -Titanium: tansig; -Aluminum: poslin;	BP; total data set: 1337		
		ANFIS Fuzzy inference System: if-then rules			

5 Digital Image Processing in Machining

DIP refers to the operations of the enhancement and or the extraction of information from digital images. Those operations are mathematical algorithms normally applied to a 2-D matrix that represents the image pixels [102]. The use of DIP techniques presumes that a digital image presents different regions, so the algorithms application highlights the regions interest (boundaries, transitions). To segment an image in regions thresholding algorithms are often used. The image grey level histogram is used to calculate a limit that distinguish the background from the foreground pixels, this process is often called binarization since the image is converted into a binary [102, 103].

A digital image can be a source of significant information about the machining outputs, such as the machined surface, the cutting tool and the chips. The use of DIP to inspect the surface integrity in machined parts was reported by authors, the covered topics included, the microstructural analysis of the surface and cross-section of machined workpieces [39, 104–106], but also the texture and topographic features related with the feed marks [100, 103, 107].

Some authors applied DIP t to measure the flank wear from digital images of the cutting tool [13, 108], while others predicted the tool wear using features extracted from digital images of the machined surfaces [9, 31, 108]. Some authors defined DIP routines to analyze the metal debris produced in machining processes, including the morphological and microstructural features of those chips [46, 53], but also the volume and shape of the removed material [32, 109].

DIP routines are suitable to analyze the alloy microstructural features such as the volume fraction of α and β phases, the grain morphology and size from digital images of the raw materials, machined parts and metal chips [42, 43, 104, 110]. This is relevant because, the thermo-mechanical properties and machinability of Ti6Al4V are related to the material microstructure [38, 41–44]. The volume fraction of the α and β phase in Ti6Al4V changes the deformation mechanism of this alloy during the machining process. Also, machining induces microstructural changes in the alloy due to high temperature at the cutting zone. DIP was used by authors [42, 43, 104] to characterize the microstructure of raw materials and machined parts. For instance, Campbell *et al.* [42, 43] developed a routine to segment and measure α grains in grey level images of Ti6Al4V microstructures. They used a watershed algorithm before thresholding to improve segmentation

accuracy. Yang [104] used a DIP routine (based on edge detection with a canny algorithm) to identify the microstructural changes during a milling process of Ti6Al4V alloy.

Some authors [9, 31, 100, 103] used DIP to extract texture features from the machined surfaces to establish relationships (using AI algorithms and mathematical models) with machining process variables such as roughness [100, 103] and tool wear [9, 31, 111]. The texture analysis in DIP consists of detecting patterns in an image, which is very useful for machined surfaces since they are characterized by feed mark patterns that change with the process conditions [112].

Texture analysis in machined surfaces obtained with different cutting conditions was performed by Kamguem [103]. The images were binarized and three algorithms, namely, gradient factor of the surface, the average cycle of texture and the average grey level were used. A set of correlation equations between the texture characteristics and the measured roughness were established. The estimated roughness using the models showed good accuracy compared with the measured values. The key finding in this research was the opportunity of measuring the surface roughness, in an indirect way, using a vision system (camera + DIP routine+ mathematical models).

Umamaheswara *et al.* [100] also worked with surface texture analysis. The authors used a support vector machine algorithm to estimate the roughness and the identify the operation (turning, face milling, milling) based on the texture features and the measured surface roughness.

Dutta *et al.* [9, 31] also used texture analysis, however, the texture features were used to predict the flank wear. The authors proposed a technique where three methods of texture analysis, grey level co-occurrence matrix (GLCM), Voronoi tessellation (VT), discrete wavelet transformation (DWT) were applied in turned surface images to extract six descriptors related to waviness, feed mark, and roughness. A supervised learning algorithm as used for data analysis and classification. To predict the progressive tool wear, the algorithm was trained using the extracted surface features and the experimental tool flank wear as the target variable. An important remark in the research conducted by these authors was that the images were acquired and processed in real-time, which is a good indication for the possibility of integrating this solution on a machine vision system for monitoring and control of the machining process.

Some authors [10, 108, 113] applied DIP to evaluate the tool, namely the tool wear. Thakre [108] develop a DIP method (thresholding, median filtering, dilation and erosion operations and canny

edge detection) to measure tool wear parameters, such as average wear width, wear area, wear perimeter.

Mikołajczyk *et al.* [10, 113] studied the tool condition for a turning operation with an unsupervised NN to detect the worn area based on the pixel brightness. The flank wear was estimated based on the number of pixels of the worn area detected by the intelligent algorithm. The estimated flank wear was compared with the one measured manually, to validate the results. The manual and the image-based flank wear measurements were applied in an ANN to predict the tool life.

Fernández-Robles *et al.* [13] proposed a computer vision system to identify broken inserts in milling operations. The DIP routine was composed of morphological operations to detect the inserts, the criterion established to decide if the insert was broken or not was the geometrical deviations between the expected cutting edge and the real cutting edge. The authors concluded the article by stating that, the proposed computer vision system has the potential to be implemented in online configurations if the insert images were acquired during the transition between operation.

DIP was also used for characterizing the metal chips from machining processes. For a Ti6Al4V turning process, Sánchez Hernández [46] evaluated the morphological aspects of the chips, namely height peak and valley, shrinkage factor, segment ratio and width, chip thickness and shear angle. A mathematical model was defined to establish relationships between the chip-parameters and the cutting parameters. Harzallah [53] also studied morphological parameters of the metal chips of Ti6Al4V, the chip-geometric features (chip length and height, shear angle, frequency of segmentation) were obtained during the machining process using a high-speed camera.

Zuperl [32, 109] developed an machining system with real-time chip size monitoring and feed rate control capabilities based on the required surface roughness. The chip volume descriptors were created by means of a machine vision system and DIP routine. The chip-descriptors were used to feed an ANFIS network in order to predict the surface roughness. The feed rate was controlled in order to maintain a constant surface roughness. Few works were found that reached this degree of adaptive process control.

5.1 Digital image processing in machining: strategies, goals & challenges

Table 7 summarizes DIP strategies for materials other than Ti6Al4V, since DIP consists in methods that can be applied in different materials.

Authors have been using DIP to analyze morphological aspects of the metal chips formed during machining processes in order to relate them with the cutting conditions [46] or to validate FEM models [53]. This task is usually performed using manual DIP [46, 53] instead of automatic DIP [32, 109, 114]. However, the manual method is more exposed to the operator observation variability than the automatic one and tends to be limited in the number of samples analyzed since it is time-consuming [115]. There is a lack of automated solutions to analyze the morphological aspects of the serrated metal chips. This represents a setback (and an opportunity) considering the requirements for the future machining systems where a large amount of data must be collected and transformed in useful information for controlling the machining process.

In Table 7 for each strategy the solution attributes, in terms of DIP technique (manual or automatic) and type of acquisition are described. To do an image-based analysis, a picture must be acquired, it could be in real-time, also called online monitoring or following the process, also called offline mode. In online monitoring, the digital images are frequently obtained through objective lens attached into a high-speed digital camera [53], while in offline mode, a similar set can be used, or the images can be captured using microscopes such as optical (OM) or electronic scan (SEM) [104]. Most digital images from Table 7 were obtained offline. While online solutions are the most relevant in the context of industry 4.0 since they can inform the current state of the machining system and process.

Table 7. DIP applied in machining process of several materials including Ti6Al4V.

	Variable/ Material	Solution attributes	Input	Image processing	Output	Other remarks
Pristine material Campbell *et al.* 2017, 2018 [42, 43]	**Ti6Al4V** Microstructure	Automated DIP; offline acquisition	SEM micrographs	Segmentation: Watershed algorithm	Grain size % α and β phase	Comparison with manual methods
Milling Yang 2016 [104]	**Ti6Al4V** Microstructure pristine material & machined part			Edge detection: Canny algorithm		Stress-strain-%β phase curve via FEM simulation
Milling & Turning Umamaheswara Raju 2017 [100]	**Mild steel** Machined surface	Automated DIP (MATLAB); offline acquisition; average arithmetic surface roughness measured with a profilometer	Machined surfaces R_{aM} [µm]	Texture feature extraction using threshold true-color RGB		SVM algorithm to predict R_a using texture features
Turning Kamguem 2013 [103]	**Al 6061** Machined surface			Binarization to extract: Gradient factor of surface; Average cycle of texture [107]; Average grey level		Correlation equations of R_a with the texture features; Comparation of estimated R_a (image) with R_{aM} (profilometer).
Turning Thakre 2019 [108]	**Low alloy steel** Tool wear	Automated DIP (MATLAB); offline acquisition; flank wear was also measured manually	V_{BM} [mm]	Binarization; Edge detection; Segmentation	Wear: width, area, perimeter	Comparison between V_B (automatic) and V_{BM} (manual)
Turning Mikołajczyk 2017, 2018 [10, 113]	**C45** Tool wear	Automated DIP; offline acquisition; prediction of tool wear and tool life using intelligent algorithms	V_{BM} [mm] Tool life [min]	Pixel brightness to define the damaged area, using an unsupervised learning algorithm; Worn area number of pixels was used to estimate the V_B and compared with the V_{BM}; An artificial neural network was used to predict tool life based on V_B		
Milling Fernández-Robles *et al.* 2017 [13]	Insert breakability	Computer vision system, automated DIP (MATLAB); offline acquisition	Images of cutting edges	Define a region of interest (and mask); edge detection		Deviations between the expected cutting edge and the real cutting edge
Turning Hernández 2018 [46]	**Ti6Al4V** Chip morphology	Manual DIP using software; offline acquisition	Metal chips	Height peak/ valley; Shrinkage factor; Segment ratio/ width; Chip thickness; Shear angle		Parametric relationships between chip descriptors and cutting conditions

Turning Dutta *et al.* 2015, 2016 [9, 31]	**AISI 1050** Tool Wear	Online acquisition surface; automated DIP (MATLAB) to extract surface features; intelligent algorithm to predict tool wear	V_{BM} [mm] Machined surfaces	Surface texture analysis: GLCM, VT, DWT	descriptors for waviness, feed marks, roughness.	SVM algorithm to predict the V_B based on the surface descriptors
Milling Zuperl 2015, 2019 [32, 109]	**16MnCr5 Steel** Chip volume	Automated DIP (MATLAB); online acquisition;	Metal chips	Binarization; Segmentation; Object detection;	number of chips; largest chip size	Based on chip geometry R_a is predicted using ANFIS; Feed rate is controlled based on expected R_a
Orthogonal Cutting 3D Harzallah 2017 [53]	**Ti6Al4V** Chip morphology	A high number of chip segments were analyzed however, the DIP methodology was not described in detail, but seems manual; online acquisition;	Metal chips	Length/height; shear angle; frequency of segmentation	The experimental chip formation process was compared with a 3D FE orthogonal cutting model.	
Micro Milling Tuiran 2018 [116]	**Ti-Cp** Burr formation	Automated DIP; offline acquisition; user interface in MATLAB	Machined samples	Binarization Burr percentage calculation based on are in pixel.	The measured values were compared with direct measurements with optical microscopy	
Orthogonal turning Hrechuk 2019 [114]	**316L stainless steel; Inconel 718;** Chip morphology	Automated DIP (MATLAB); offline acquisition;	Metal chips	Mean chip thickness based on peak and valley analysis;	Shape factor to measure the material deformation. Cumulative distribution function for peaks and valley was helpful to quantify the transition of continuous to segmented chips for different feed rates.	

R_{aM}: average arithmetic roughness measured with profilometer; V_{BM}: Tool flank wear when is measured manually; RGB: Red Blue Green; V_B: Tool flank wear; GLCM: Gray level co-occurrence matrix; VT: Voronoi tessellation; DWT: Discrete wavelet transformation; FEM: Finite Element Method; R_a: average arithmetic roughness; SVM: Support Vector Machine;

6 Conclusions and outlook

Intelligence in machining operations will come from the system knowledge about aspects of the, machine center dynamics, workpiece material, the cutting parameters, the chip-tool contact conditions, the cutting tools, the cutting environment along with the process response in terms of machined part, the generated metal chips, the in-process measurements. If the machining system has access to data that allows it to understand its current state and the ideal working condition (considering the component, the productivity and sustainability requirements), that system will be able to decide regarding the process.

This will certainly involve the integration of machining information in databases, including models that correlate the entrance and response variables relevant for each industrial sector. Additionally, computer systems work and communicate though digital data and several promising modelling and optimization techniques (including artificial intelligence and machine learning) rely on process digital data to be parametrized, which means that future machining research must be focused on finding ways of collect (using conventional sensors, smart cutting tools, digital images, machine vision systems), convert to digital and quantifying the machining response to be used in modelling and optimization of cutting operations.

The aim of the article was to present an overview of the computational and digital methodologies (FEM, AI-Based models, DIP) used by researchers to model and quantify the machining response in an alloy that presents specific machining challenges. The scientifical value of the article is, above all, in the demonstration that the work presented by field researchers must be observed in an integrated way, which means that, future researcher in field must not only generate new knowledge but should be also integrated in the global context (smart machining systems). Table 8 contains examples of research works that culminate in the development of smart cutting strategies, with adaptive control of the machining process and smart cutting tools, where the methodologies (for process modelling and quantification of machining response) adopted by the researchers are highlighted.

Table 8. Smart cutting tools and smart machining techniques.

Operation; Material; Author	Aim & Techniques & Technologies involved	Contribution for smart machining
Turning Stainless Steel Huang 2020 [24]	**SCT** with optical fiber sensors for cutting force measurement, a dynamometer was used for calibration; **FEM** was used to **model** and calibrate the sensor in terms of force measurement; Comparative cutting **experiments** were performed with new sensor and dynamometer.	Real-time and multi-point cutting force measurement; Low cost.
Zhao 2018 [25]	**SCT** base on micro-electro-mechanical system strain gauge, for cutting force measurement; Sensor characterization: sensitivity and accuracy	Compact tool; No cutting tests were performed.
Turning Al 6082 Wang 2013 [26]	**SCT** with a piezoelectric film for force measurement, a dynamometer was used for calibration; Feed-surface speed-force **model** to select the constraint variable; **AC** of feed rate to keep the main the cutting force constant; If the current state is not acceptable, the lathe parameters are updated with the optimal cutting parameters.	Compact, self-monitoring tool; User interface: current-optimal regime, algorithms for **optimization** and **actuation;** Adaptative machining using SCT; Lathe with AC; Interconnection between process and machine.
Turning Steel-Monel Wang 2014 [27]	**SCT** with surface acoustic wave (SAW) strain sensors mounted in two location of the tool shank to measure cutting and feed force; Sensor characterization and comparison with dynamometer; **AC** of feed rate to keep the main the cutting force constant during machining of dissimilar materials.	
Turning Stainless steel Karam 2015 [117]	**Multi-sensor** assisted machining: cutting force, vibration, and acoustic emission sensor; **Signal processing** (feature extraction and patterns recognition) to build **sensorial database; Decision making system** for tool wear assessment via **neural network** (input: signal features, output: consumed tool life); Network was trained with tool wear measurements obtained with a **microscope;** When maximum tool wear is reached a warning is sent to change the cutting tool.	**Real-time** tool condition monitoring system; **Online** cutting tool life assessment; Pre-failure assessment system; Lathe with **AC**.
Milling Steel Zuperl 2015, 2019 [32, 109]	**Digital image processing** to obtain average chip size (CSA) in real-time; Surface roughness was predicted using an **ANFIS** model (input: CSA, radial and axial depth of cut, feed rate, cutting speed, output: surface roughness); Network was trained with surface roughness values measured with roughness tester; **AC** to adjust the feed rate to maintain surface roughness.	**Online** vision system for chip size evaluation; CNC machine with feed rate **AC**.
Drilling CFRP Hassan 2018 [34]	Signal processing techniques (acoustic emission signals, force, vibration); Force-wear database; Decision making system (online), to adapt the feed rate considering the tool wear; **AC** to adjust feed rate.	Sensitive to changes in tool condition (crack propagation, chipping/breakage); Signal processing and decision making in appropriate time span.

SCT: smart cutting tool; AC: adaptive control

If in the past, many experimental setups have been created exclusively for machining model creation, the current and future trend will certainly be use (and develop) techniques and tools to collect information from manufacturing systems that work daily and represent the real machining scenarios that industries face every day. This step will be crucial to guarantee that the efforts from the scientifical and industrial sectors are aligned in the construction of future machining systems.

It is important to emphasize that the industrial machining sector demands methodologies that can be easily implemented for the tasks they execute daily and with direct outputs, such as the tool condition state and life, the machined surface integrity, the optimized cutting conditions, and others. So, for the future, it is important that researchers continue on working in solutions (including machining process models, smart cutting tools), that ultimately led to the prediction and control of such variables.

Through this review, it was possible to recognize that process data concerning Ti6Al4V machining can be collected and analyzed with a variety of methodologies (empirical, numerical, analytical, statistical, AI-based models) that complement and validate each other (hybrid approach) and open the possibility to create machining systems with self-optimization skills.

The modeling techniques, namely FEM and AI-based are crucial in the context of intelligence in machining process as they are intrinsically intelligent techniques that can predict the system response in machining processes. Modeling with FEM is especially useful to understand the physical phenomena that occur in machining, which is even more valuable when machining Ti6Al4V which presents a peculiar behavior when being machined, namely the formation of chips with serrated morphology. However, there are a higher number of FEM models that estimate fundamental machining variables than outputs with industrial interest. Either way, the data from these simulations are often used to enter data in other types of models such as analytical or even to validate new analytical models. For example, variables calculated with FEM (strain, cutting forces) have been used to validate chip formation models in orthogonal cutting [81], the state variables at the tool face calculated with FEM have been used to determine the constants at tool wear models [85]. This tendency to use hybrid numerical- empirical and numerical-analytical models can be useful to reduce the computational time and create more complex models able to calculate machining responses with higher industrial interest. Most AI-based models describe in

this review were able to predict response variables with industrial interest, such as surface roughness and tool wear.

DIP proved to be a technique that integrated into machine vision systems can be able to monitor in-process machining operations in terms of tool condition and surface quality. This approach is often associated with AI algorithms capable to predict machining outputs based in digital image features.

It seems that the development of intelligent machining solutions should depend on hybrid models that integrate different approaches to take advantage of the benefits presented by every single technique. The processing by machining of difficult to cut material is one of the areas where the hybrid approach can bring greater socio-economic benefit.

Acknowledgments: The authors acknowledge “Project No. 031556-FCT/02/SAICT/ 2017; FAMASI - Sustainable and intelligent manufacturing by machining, financed by the Foundation for Science and Technology (FCT), POCI, Portugal, in the scope of TEMA, Centre for Mechanical Technology and Automation - UID/EMS/00481/2013.

References

[1] Byrne G, Ahearne E, Cotterell M, et al. High Performance Cutting (HPC) in the New Era of Digital Manufacturing – A Roadmap. In: *Procedia CIRP*. Elsevier B.V., pp. 1–6.

[2] Ahuett-Garza H, Kurfess T. A brief discussion on the trends of habilitating technologies for Industry 4.0 and Smart manufacturing. *Manuf Lett* 2018; 15: 60–63.

[3] Yang S, M. R. A, Kaminski J, et al. Opportunities for Industry 4.0 to Support Remanufacturing. *Appl Sci* 2018; 8: 1177.

[4] Deb S, Dixit US. Intelligent machining: Computational methods and optimization. In: *Machining: Fundamentals and Recent Advances*. London: Springer, pp. 329–358.

[5] Arrazola PJ, Özel T, Umbrello D, et al. Recent advances in modelling of metal machining processes. *CIRP Ann - Manuf Technol* 2013; 62: 695–718.

[6] Lauro CH, Brandão LC, Filho SLMR, et al. Finite Element Method in Machining Processes: A Review. In: Davim JP (ed) *Modern Manufacturing Engineering*. Springer, pp. 65–97.

[7] Pradhan S, Singh S, Prakash C, et al. Investigation of machining characteristics ofhard-to-machine Ti-6Al-4V-ELI alloy for biomedicalapplications. *J Mater Res Technol* 2019; 8: 4849–4862.

[8] Shan C, Zhang M, Zhang S, et al. Prediction of machining-induced residual stress in orthogonal cutting of Ti6Al4V. *Int J Adv Manuf Technol* 2020; 107: 2375–2385.

[9] Dutta S, Pal SK, Sen R. On-machine tool prediction of flank wear from machined surface images using texture analyses and support vector regression. *Precis Eng* 2016; 43: 34–42.

[10] Mikołajczyk T, Nowicki K, Bustillo A, et al. Predicting tool life in turning operations using neural networks and image processing. *Mech Syst Signal Process* 2018; 104: 503–513.

[11] Quiza R, Davim JP. Combining Finite Element Method and Artificial Intelligence in Manufacturing Modeling and Optimization. In: *Finite Element Method in Manufacturing Processes*. 2010, pp. 2001–236.

[12] Kim DH, Kim TJY, Wang X, et al. Smart Machining Process Using Machine Learning: A Review and Perspective on Machining Industry. *Int J Precis Eng Manuf - Green Technol* 2018; 5: 555–568.

[13] Fernández-Robles L, Azzopardi G, Alegre E, et al. Machine-vision-based identification of broken inserts in edge profile milling heads. *Robot Comput Integr Manuf* 2017; 44: 276–283.

[14] Altintas Y. *Manufacturing Automation: Metal Cutting Mechanics, Machine Tool Vibrations, and CNC Design*. Cambridge University Press, 2012.

[15] Cheng K (ed). *Machining Dynamics: Fundamentals, Applications and Practices*. London: Springer, 2009. Epub ahead of print 2009. DOI: 10.1007/978-1-84628-368-0.

[16] Kovač P, Mankova I. A review of machining monitoring systems. *J Prod …* 2011; 11: 8–13.

[17] Lauro CH, Brandão LC, Baldo D, et al. Monitoring and processing signal applied in machining processes - A review. *Meas J Int Meas Confed* 2014; 58: 73–86.

[18] Caggiano A. Tool wear prediction in Ti-6Al-4V machining through multiple sensor monitoring and PCA features pattern recognition. *Sensors (Switzerland)*; 18. Epub ahead of print 2018. DOI: 10.3390/s18030823.

[19] Wang Z, Nakashima S, Larson M. Energy Efficient Machining of Titanium Alloys by Controlling Cutting Temperature and Vibration. *Procedia CIRP* 2014; 17: 523–528.

[20] Barry J, Byrne G, Lennon D. Observations on chip formation and acoustic emission in machining Ti-6Al-4V alloy. *Int J Mach Tools Manuf* 2001; 41: 1055–1070.

[21] Mane S, Ramchandani J, Marla D, et al. Experimental investigation of oil mist assisted cooling on orthogonal cutting of Ti6Al4V. *Procedia Manuf* 2019; 34: 369–378.

[22] Joshi S. Dimensional inequalities in chip segments of titanium alloys. *Eng Sci Technol an Int J* 2018; 21: 238–244.

[23] Joshi S, Tewari A, Joshi SS. Microstructural characterization of chip segmentation under different machining environments in orthogonal machining of Ti6Al4V. *J Eng Mater Technol Trans ASME* 2015; 137: 011005:1–16.

[24] Huang J, Pham DT, Ji C, et al. Smart Cutting Tool Integrated with Optical Fiber Sensors for Cutting Force Measurement in Turning. *IEEE Trans Instrum Meas* 2020; 69: 1720–1727.

[25] Zhao Y, Zhao YL, Shao YW, et al. Research of a smart cutting tool based on MEMS strain gauge. *J Phys Conf Ser*; 986. Epub ahead of print 2018. DOI: 10.1088/1742-6596/986/1/012016.

[26] Wang C, Ghani SBC, Cheng K, et al. Adaptive smart machining based on using constant cutting force and a smart cutting tool. *Proc Inst Mech Eng Part B J Eng Manuf* 2013; 227: 249–253.

[27] Wang C, Cheng K, Chen X, et al. Design of an instrumented smart cutting tool and its implementation and application perspectives. *Smart Mater Struct*; 23. Epub ahead of print 2014. DOI: 10.1088/0964-1726/23/3/035019.

[28] Dutta S, Pal SK, Sen R. Digital Image Processing in Machining. In: Davim JP (ed) *Modern*

Mechanical Engineering. Berlin, Heidelberg: Springer Berlin Heidelberg, pp. 367–410.

[29] Nouari M, Makich H. On the Physics of Machining Titanium Alloys: Interactions between Cutting Parameters, Microstructure and Tool Wear. *Metals (Basel)* 2014; 4: 335–358.

[30] Hughes JI, Sharman ARC, Ridgway K. The effect of cutting tool material and edge geometry on tool life and workpiece surface integrity. *Proc Inst Mech Eng Part B J Eng Manuf* 2006; 220: 93–107.

[31] Dutta S, Pal SK, Sen R. Tool Condition Monitoring in Turning by Applying Machine Vision. *J Manuf Sci Eng* 2015; 138: 051008.

[32] Župerl U, Čuš F. A Cyber-Physical System for Surface Roughness Monitoring in End-Milling. *Strojniški Vestn – J Mech Eng* 2019; 65: 67–77.

[33] Kaplan A, Haenlein M. Siri, Siri, in my hand: Who's the fairest in the land? On the interpretations, illustrations, and implications of artificial intelligence. *Bus Horiz* 2019; 62: 15–25.

[34] Hassan M, Sadek A, Attia MH, et al. Intelligent machining: Real-Time Tool Condition Monitoring And Intelligent Adaptative Control Systems. *J Mach Eng* 2018; 18: 5–18.

[35] Veiga C, Davim JP, Loureiro AJR. Properties and applications of titanium alloys: A brief review. *Rev Adv Mater Sci* 2012; 32: 133–148.

[36] Ortiz-de-Zarate G, Madariaga A, Garay A, et al. Experimental and FEM analysis of surface integrity when broaching Ti64. In: *Procedia CIRP*. Elsevier B.V., pp. 466–471.

[37] Zhang XP, Shivpuri R, Srivastava AK. Role of phase transformation in chip segmentation during high speed machining of dual phase titanium alloys. *J Mater Process Technol* 2014; 214: 3048–3066.

[38] Peters M, Leyens C. *Titanium and Titanium Alloys Fundamentals and Applications*. WILEY-VCH. Epub ahead of print 2003. DOI: 10.1002/3527602119.

[39] Sun Y, Huang B, Puleo DA, et al. Improved Surface Integrity from Cryogenic Machining of Ti-6Al-7Nb Alloy for Biomedical Applications. In: *Procedia CIRP*. Elsevier B.V., pp. 63–66.

[40] Pramanik A. Problems and solutions in machining of titanium alloys. *Int J Adv Manuf Technol* 2014; 70: 919–928.

[41] Sun SJ, Brandt M, Mo JPT. Effect of Microstructure on Cutting Force and Chip Formation during Machining of Ti-6Al-4V Alloy. *Adv Mater Res* 2013; 690–693: 2437–2441.

[42] Campbell A, Murray P, Yakushina E, et al. Automated microstructural analysis of titanium alloys using digital image processing. In: *IOP Conference Series: Materials Science and Engineering*, p. 012011.

[43] Campbell A, Murray P, Yakushina E, et al. New methods for automatic quantification of microstructural features using digital image processing. *Mater Des* 2018; 141: 395–406.

[44] Patil S, Kekade S, Phapale K, et al. Effect of α and β Phase Volume Fraction on Machining Characteristics of Titanium Alloy Ti6Al4V. *Procedia Manuf* 2016; 6: 63–70.

[45] Ducobu F, Rivière-Lorphèvre E, Filippi E. Numerical contribution to the comprehension of saw-toothed Ti6Al4V chip formation in orthogonal cutting. *Int J Mech Sci* 2014; 81: 77–87.

[46] Sánchez Hernández Y, Trujillo Vilches F, Bermudo Gamboa C, et al. Experimental Parametric Relationships for Chip Geometry in Dry Machining of the Ti6Al4V Alloy. *Materials (Basel)* 2018; 11: 1260–1277.

[47] Zhang Y, Outeiro JC, Mabrouki T. On the selection of Johnson-Cook constitutive model parameters for Ti-6Al-4V using three types of numerical models of orthogonal cutting. In: *Procedia CIRP*. Elsevier B.V., pp. 112–117.

[48] Parida AK. Simulation and experimental investigation of drilling of Ti-6Al-4V alloy. *Int J Light Mater Manuf* 2018; 1: 197–205.

[49] Calamaz M, Coupard D, Girot F. A new material model for 2D numerical simulation of serrated chip formation when machining titanium alloy Ti–6Al–4V. *Int J Mach Tools Manuf* 2008; 48: 275–288.

[50] Li A, Pang J, Zhao J, et al. FEM-simulation of machining induced surface plastic deformation and microstructural texture evolution of Ti-6Al-4V alloy. *Int J Mech Sci* 2017; 123: 214–223.

[51] Johnson GR, Cook WH. A constituive Model and Data for Metals Subjected to High Strains, High Strain Rates, Temperatures and Pressures. In: *Proceedings of the 7th International Symposium on Ballistics*. Hague, Netherlands, 1983, pp. 541–547.

[52] Sima M, Özel T. Modified material constitutive models for serrated chip formation simulations and experimental validation in machining of titanium alloy Ti-6Al-4V. *Int J Mach Tools Manuf* 2010; 50: 943–960.

[53] Harzallah M, Pottier T, Senatore J, et al. Numerical and experimental investigations of Ti-6Al-4V chip generation and thermo-mechanical couplings in orthogonal cutting. *Int J Mech Sci* 2017; 134: 189–202.

[54] Marusich TD, Ortiz M. Modelling and simulation of high-speed machining. *Int J Numer Methods Eng* 1995; 38: 3575–3694.

[55] Bajpai V, Lee I, Park HW. Finite Element Modeling of Three-Dimensional Milling Process of Ti–6Al–4V. *Mater Manuf Process* 2014; 29: 564–571.

[56] Ji C, Li Y, Qin X, et al. 3D FEM simulation of helical milling hole process for titanium alloy Ti-6Al-4V. *Int J Adv Manuf Technol* 2015; 81: 1733–1742.

[57] Lesuer DR. *Experimental Investigations of Material Models for Ti6Al4V Titanium and 2024-T3 Aluminum*, papers2://publication/uuid/31CAFE5C-D94D-4AC7-A7E0-87F63BF4C74A (2000).

[58] Lee WS, Lin CF. High-temperature deformation behaviour of Ti6A14V alloy evaluated by high strain-rate compression tests. *J Mater Process Technol* 1998; 75: 127–136.

[59] Özel T, Karpat Y. Identification of constitutive material model parameters for high-strain rate metal cutting conditions using evolutionary computational algorithms. *Mater Manuf Process* 2007; 22: 659–667.

[60] Khan AS, Suh YS, Kazmi R. Quasi-static and dynamic loading responses and constitutive modeling of titanium alloys. *Int J Plast* 2004; 20: 2233–2248.

[61] LÖSCHNER P, JAROSZ K, NIESŁONY P. OPTIMIZATION OF JOHNSON–COOK CONSTITUTIVE MODEL PARAMETERS. *Eng Mech Eng Manuf* 2019; 19: 66–73.

[62] Hou X, Liu Z, Wang B, et al. Stress-strain curves and modified material constitutive model for Ti-6Al-4V over thewide ranges of strain rate and temperature. *Materials (Basel)*; 11. Epub ahead of print 2018. DOI: 10.3390/ma11060938.

[63] Gu XY, Dong CY, Cheng T. MPM simulations of high-speed machining of Ti6Al4V titanium alloy considering dynamic recrystallization phenomenon and thermal conductivity. *Appl Math Model* 2018; 56: 517–538.

[64] Melkote S, Grzesik W, Outeiro J, et al. Advances in material and friction data for modelling of metal machining. *CIRP Ann - Manuf Technol* 2017; 66: 731–754.

[65] Cockcroft MG, Latham DJ. Ductility and the workability of metals. *J Inst Met*; 96.

[66] Sekar KSV, Kumar MP. Finite element simulations of Ti6Al4V titanium alloy machining to assess material model parameters of the Johnson-Cook constitutive equation. *J Brazilian Soc Mech Sci Eng* 2011; 33: 203–211.

[67] Chiappini E, Tirelli S, Albertelli P, et al. On the mechanics of chip formation in Ti- 6Al-4V turning with spindle speed variation. *Int J Mach Tools Manuf* 2014; 77: 16–26.

[68] Syed K. *Finite Element Simulation of chip segmentation in machining a Ti-6Al-4V alloy*. 2004.

[69] Li N, He N. A FEA study on mechanisms of saw-tooth chip deformation in high speed cutting of Ti–6–Al–4V alloy. In: *Fifth International Conference on High Speed Machining (HSM)*. Metz, France, 2006, pp. 759–767.

[70] Özel T, Zeren E. Determination of work material flow stress and friction for FEA of machining using orthogonal cutting tests. *J Mater Process Technol* 2004; 153–154: 1019–1025.

[71] Sun J, Guo YB. Material flow stress and failure in multiscale machining titanium alloy Ti-6Al-4V. *Int J Adv Manuf Technol* 2009; 41: 651–659.

[72] Niesłony P, Grzesik W, Habrat W. Experimental and simulation investigations of face milling process of Ti-6Al-4V titanium alloy. *Adv Manuf Sci Technol* 2015; 39: 39–52.

[73] Niesłony P, Grzesik W, Laskowski P, et al. Numerical and experimental analysis of

residual stresses generated in the machining of Ti6A14V titanium alloy. *Procedia CIRP* 2014; 13: 78–83.

[74] Childs THC. Friction modelling in metal cutting. *Wear* 2006; 260: 310–318.

[75] Raza SW, Pervaiz S, Deiab I. Tool Wear Patterns When Turning of Titanium Alloy Using Sustainable Lubrication Strategies. *Int J Precis Eng Manuf* 2014; 15: 1979–1985.

[76] Yan P, Rong Y, Wang G. The effect of cutting fluids applied in metal cutting process. *Proc Inst Mech Eng Part B J Eng Manuf* 2016; 230: 19–37.

[77] Chen G, Chen S, Caudill J, et al. Effect of cutting edge radius and cooling strategies on surface integrity in orthogonal machining of Ti-6Al-4V alloy. *Procedia CIRP* 2019; 82: 148–153.

[78] Özel T. The influence of friction models on finite element simulations of machining. *Int J Mach Tools Manuf* 2006; 46: 518–530.

[79] Zorev N. Interrelationship between shear processes occurring along tool face and on shear plane in metal cutting. *ASME Proc Int Res Prod Eng* 1963; 42.

[80] Özel T, Sima M, Srivastava AK, et al. Investigations on the effects of multi-layered coated inserts in machining Ti-6Al-4V alloy with experiments and finite element simulations. *CIRP Ann - Manuf Technol* 2010; 59: 77–82.

[81] Bai W, Sun R, Roy A, et al. Improved analytical prediction of chip formation in orthogonal cutting of titanium alloy Ti6Al4V. *Int J Mech Sci* 2017; 133: 357–367.

[82] Ducobu F, Rivière-Lorphèvre E, Filippi E. Influence of the material behavior law and damage value on the results of an orthogonal cutting finite element model of Ti6Al4V. *Procedia CIRP* 2013; 8: 379–384.

[83] Ren C, Ke Z, Chen G, et al. Modeling of tool-chip contact length for orthogonal cutting of Ti-6Al-4V alloy considering segmented chip formation. *Trans Tianjin Univ* 2016; 22: 525–535.

[84] Usui E, Shirakashi T, Kitagawa T. Analytical prediction of three dimensional cutting process: Part 3 cutting temperature and crater wear of carbide tool. *J Manuf Sci Eng Trans*

ASME 1978; 100: 236–243.

[85] Zanger F, Schulze V. Investigations on Mechanisms of Tool Wear in Machining of Ti-6Al-4V Using FEM Simulation. *Procedia CIRP* 2013; 8: 158–163.

[86] Recht R. Catastrophic thermoplastic shear. *Trans ASME 31*; 186.

[87] Molinari A, Musquar C, Sutter G. Adiabatic shear banding in high speed machining of Ti-6Al-4V: Experiments and modeling. *Int J Plast* 2002; 18: 443–459.

[88] López De Lacalle LN, Pérez J, Llorente JI, et al. Advanced cutting conditions for the milling of aeronautical alloys. *J Mater Process Technol* 2000; 100: 1–11.

[89] Sun S, Brandt M, Dargusch MS. Characteristics of cutting forces and chip formation in machining of titanium alloys. *Int J Mach Tools Manuf* 2009; 49: 561–568.

[90] Mello G D', P SP, Shetty RP. Surface roughness modeling in high speed turning of Ti-6Al-4V – Artificial Neural Network approach. In: *Materials Today: Proceedings*. Elsevier Ltd, pp. 7654–7664.

[91] Harsha N, Kumar IA, Raju KSR, et al. Prediction of Machinability characteristics of Ti6Al4V alloy using Neural Networks and Neuro-Fuzzy techniques. In: *Materials Today: Proceedings*. Elsevier Ltd, pp. 8454–8463.

[92] Kannan TDB, Kannan GR, Kumar BS, et al. Application of Artificial Neural Network Modeling for Machining Parameters Optimization in Drilling Operation. In: *Procedia Materials Science*, pp. 2242–2249.

[93] Upadhyay V, Jain PK, Mehta NK. In-process prediction of surface roughness in turning of Ti–6Al–4V alloy using cutting parameters and vibration signals. *Measurement* 2013; 46: 154–160.

[94] Rajaparthiban J, Sait AN. Experimental Investigation on Machining of Titanium Alloy (Ti6Al 4V) and Optimization of its Parameters using ANN. *Mechanika* 2018; 24: 449–455.

[95] Mohd Adnan MRH, Sarkheyli A, Mohd Zain A, et al. Fuzzy logic for modeling machining process: a review. *Artif Intell Rev* 2015; 43: 345–379.

[96] Kumar BS, Baskar N. Integration of fuzzy logic with response surface methodology for thrust force and surface roughness modeling of drilling on titanium alloy. *Int J Adv Manuf Technol* 2013; 65: 1501–1514.

[97] Özkan G, İnal M. Comparison of neural network application for fuzzy and ANFIS approaches for multi-criteria decision making problems. *Appl Soft Comput* 2014; 24: 232–238.

[98] Eduardo C, Cruz D, Aguiar PR De, et al. Monitoring in precision metal drilling process using multi-sensors and neural network. *Int J Adv Manuf Technol* 2013; 66: 151–158.

[99] M. Geronimo T, D. Cruz CE, Souza Campos F de, et al. MLP and ANFIS Applied to the Prediction of Hole Diameters in the Drilling Process. In: *Artificial Neural Networks - Architectures and Applications*. IntechOpen, pp. 145–173.

[100] Umamaheswara Raju RS, Ramachandra Raju V, Ramesh R. Intelligence model based machining process classification and performance estimation. *Mater Today Proc* 2017; 4: 982–990.

[101] Quiza R, Davim JP. Combining the Finite Element Method and Artificial Intelligence in Manufacturning Modeling and Optimization. In: Davim JP (ed) *Finite Element Method in Manufacturing Processes*. WILEY-VCH, 2011, pp. 201–239.

[102] Sundararajan D. *Digital Image Processing: A signal Processing and Algorithmic Approach*. Singapore: Springer Singapore. Epub ahead of print 2017. DOI: 10.1007/978-981-10-6113-4.

[103] Kamguem R, Tahan SA, Songmene V. Evaluation of machined part surface roughness using image texture gradient factor. *Int J Precis Eng Manuf* 2013; 14: 183–190.

[104] Yang D, Liu Z. Quantification of Microstructural Features and Prediction of Mechanical Properties of a Dual-Phase Ti-6Al-4V Alloy. *Materials (Basel)* 2016; 9: 1–14.

[105] Arisoy YM, Özel T. Prediction of machining induced microstructure in Ti-6Al-4V alloy using 3-D FE-based simulations: Effects of tool micro-geometry, coating and cutting conditions. *J Mater Process Technol* 2015; 220: 1–26.

[106] Rotella G, Dillon OW, Umbrello D, et al. The effects of cooling conditions on surface integrity in machining of Ti6Al4V alloy. *Int J Adv Manuf Technol* 2014; 71: 47–55.

[107] Jian Z, Jin Z. Surface roughness measure based on average texture cycle. *Proc - 2010 2nd Int Conf Intell Human-Machine Syst Cybern IHMSC 2010* 2010; 2: 298–302.

[108] Thakre AA, Lad A V., Mala K. Measurements of Tool Wear Parameters Using Machine Vision System. *Model Simul Eng* 2019; 2019: 1–9.

[109] Zuperl U, Cus F. Simulation and visual control of chip size for constant surface roughness. *Int J Simul Model* 2015; 14: 392–403.

[110] Joshi S, Pawar P, Tewari A, et al. Effect of β phase fraction in titanium alloys on chip segmentation in their orthogonal machining. *CIRP J Manuf Sci Technol* 2014; 7: 191–201.

[111] Keshari A, Teti PR. *Advanced Techniques for Monitoring , Simulation and Optimization of Machining Processes*. 2011.

[112] Dutta S, Pal SK, Mukhopadhyay S, et al. Application of digital image processing in tool condition monitoring: A review. In: *CIRP Journal of Manufacturing Science and Technology*. Elsevier, pp. 212–232.

[113] Mikołajczyk T, Nowicki K, Kłodowski A, et al. Neural network approach for automatic image analysis of cutting edge wear. *Mech Syst Signal Process* 2017; 88: 100–110.

[114] Hrechuk A, Bushlya V, M'Saoubi R, et al. Quantitative analysis of chip segmentation in machining using an automated image processing method. *Procedia CIRP* 2019; 82: 314–319.

[115] Chanou A, Osinski GR, Grieve RAF. A methodology for the semi-automatic digital image analysis of fragmental impactites. *Meteorit Planet Sci* 2014; 49: 621–635.

[116] Tuiran R, Onate J, Romero N. Analysis of burr formation by image processing in micro-milling of Ti. *Contemp Eng Sci* 2018; 11: 2297–2306.

[117] Karam S, Centobelli P, D'Addona DM, et al. Online Prediction of Cutting Tool Life in Turning via Cognitive Decision Making. *Procedia CIRP* 2016; 41: 927–932.